Prediction of Two-Point Statistics on Cones in High-Speed Flow via Instability Wave Theory

Jianhui Cheng and Steven A. E. Miller
University of Florida
AIAA, Jan 3-7

Acknowledgements

The authors are grateful for continuous funding from Space Research Initiative (SRI) OR-DRPD-SRI2020: Reduction of Rocket Vibrations via Control of Large-Scale Coherent Turbulent Structures.

Outline

- Introduction and Background
- Methodology
  - Instability Wave Theory
  - Cross-Power Spectral Density of Pressure from Instability Waves
- Results and Analysis
  - Flow-Field Computation and Validation
  - Stability Computation and Validation
  - Pressure Spectrum
  - Spatial Coherence
- Summary and Conclusion

Background

Fig 1. Launch of Orbital ATK's Antares rocket[1].

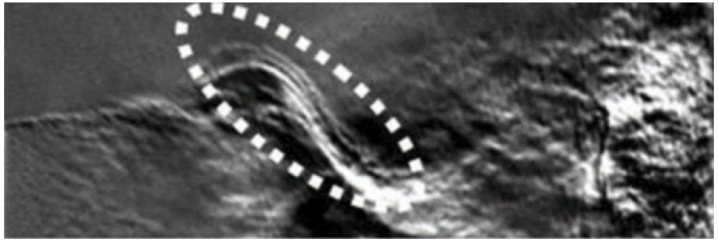

Fig 2. A schlieren of jet moving left to right where a large instability wave is circled. Courtesy of Prof. Mitchell.

- Aerodynamic loading on the flight-vehicle surface causes intensive vibration and cabin noise
- Instability waves that lead to transition to turbulence create large pressure fluctuations on the surface of vehicles
- Nose bluntness affect the stability and transition
- Objective: to further study the effects of nose bluntness within high-speed boundary layer flows via computing the pressure fluctuations from the instability waves on cones with different nose radii

[1] Lubert, C. P., "Sixty Years of Launch Vehicle Acoustics," Acoustic Society of America, Vol. 31, 2017.

Instability Wave Theory

Governing Equations[2]

$$\frac{\partial \rho}{\partial t} + \nabla \cdot (\rho u) = 0$$

$$\rho\left[\frac{\partial u}{\partial t} + (u \cdot \nabla)u\right] = -\nabla p + \nabla \cdot [\lambda(\nabla \cdot u)I] + \nabla \cdot [\mu(\nabla u + \nabla u^{tr})]$$

$$\rho c_p\left[\frac{\partial T}{\partial t} + (u \cdot \nabla)T\right] = -\nabla \cdot (k\nabla T) + \frac{\partial p}{\partial t} + (u \cdot \nabla)p + \Phi$$

Procedure

- Linearize: $u = \bar{u} + \tilde{u}, T = \bar{T} + \tilde{T}$,etc.
- Nondimensional: edge value, $l = \sqrt{\nu_e^* x^* / u_e^*}$
- Parallel flow: $\bar{u} = \bar{u}(y), \bar{T} = \bar{T}(y)$, etc.
- Sutherland law: $\bar{\mu} = \bar{T}^{3/2}\frac{1+C/T_\infty^*}{\bar{T}+C/T_\infty^*}$
- $\tilde{k} = \frac{d\bar{k}}{d\bar{T}}\tilde{T}$

Instability Wave Formula

$$\tilde{\phi}(x, y, z, t) = \hat{\phi}(y)\exp(i(\alpha x + \beta z - \omega t))$$

- α, β are the wavenumber
- $\hat{\phi}(y)$ is shape function

Linear Stability Equations System

$$\left(A\frac{d^2}{dy^2} + B\frac{d}{dy} + C\right)\hat{\phi} = 0$$

- Boundary conditions

  $y = 0,\ \hat{\phi}_1 = \hat{\phi}_2 = \hat{\phi}_3 = \hat{\phi}_5 = 0$

  $y \to \infty, \hat{\phi}_1, \hat{\phi}_2, \hat{\phi}_3, \hat{\phi}_5 \to 0$

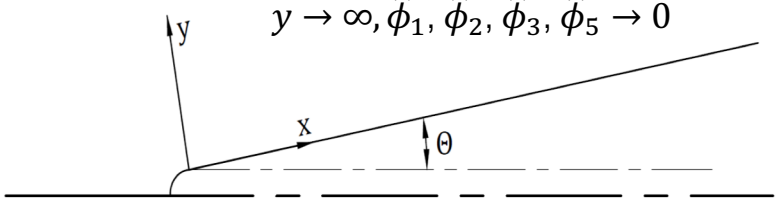

Fig 3. Coordinate system.

Cross-Power Spectral Density of Pressure from Instability Waves

- Wall Pressure Fluctuations Construction[3]

$$\tilde{p}(x,y,z,t) = \int_{-\infty}^{\infty} \hat{p}(y)\exp[i(\alpha x + \beta z - \omega t)]d\omega$$

Maximum growth rate at azimuthal direction is chosen.

- Spatial Coherence

$$\Gamma(\boldsymbol{\xi},\omega) = \frac{1}{2\pi}\int_{-\infty}^{\infty} \langle \tilde{p}(\boldsymbol{x},t), \tilde{p}(\boldsymbol{x}+\boldsymbol{\xi}, t+\tau)\rangle \exp(-i\omega\tau)\, d\tau$$

- Cross-Power Spectral Density (CPSD)[4]

$$\Psi_{pp}(\xi,\omega) = \phi(\omega)\Gamma(\xi,\omega)$$

[2] Malik, M. R., and Spall, R. E., "On the Stability of Compressible Flow Past Axisymmetric Bodies," Journal of Fluid Mechanics Digital Archive, Vol. 228, 1991, pp. 443–463.
[3] Zhou, H., "Coherent Structure Modeling and its Role in the Computation of Passive Quantity Transport in Turbulent Flows." JSME International Journal Series B, Vol. 41, No. 1, 1998, pp. 137–144.
[4] Caiazzo, A., D'Amico, R., and Desmet, W., "Use of a Generalized Corcos Model to Predict Flow-Induced Noise in a Cavity-Plate System," Proceedings of the 27th International Conference on Noise and Vibration Engineering, ISMA2016 & USD2016, 2016,pp. 1319–1332.

Mean Flow-Field

- Flow Conditions[5]

M_∞	T_∞(K)	ρ_∞(kg/m^3)	Re(1/m)	L(m)	r_n(mm)
3.5	90.1	0.0874	9.45×10^6	0.3556	0.038

- Cone Configuration and Grid Distribution

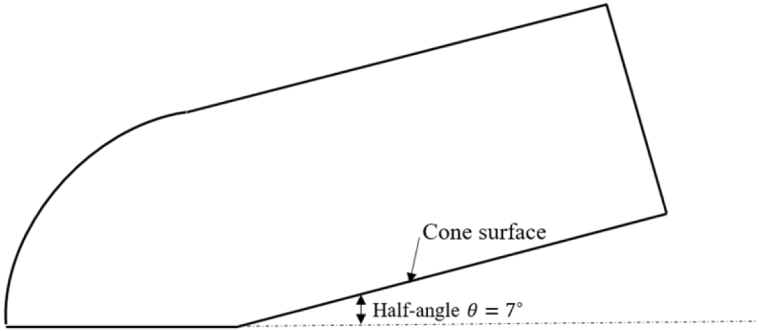

Fig 4. Flow region.

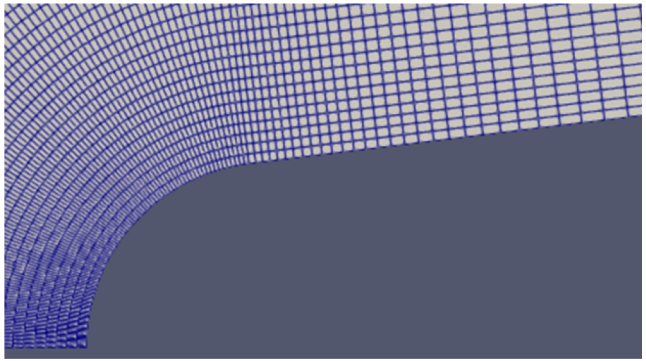

Fig 5. Nose region.

[5]Gross, A., and Fasel, H. F., "Numerical Investigation of Supersonic Flow for Axisymmetric Cones," Mathematics and Computer sin Simulation, Vol. 81, No. 1, 2010, pp. 133–142.

Mean Flow-Field

Velocity and Temperature Distribution

The Stanford University Unstructured (SU2) open-source software suite[6]

Axisymmetric; No-penetration and no-slip conditions; Adiabatic wall

Grid size in normal direction: 201 (coarse) vs 401(fine)

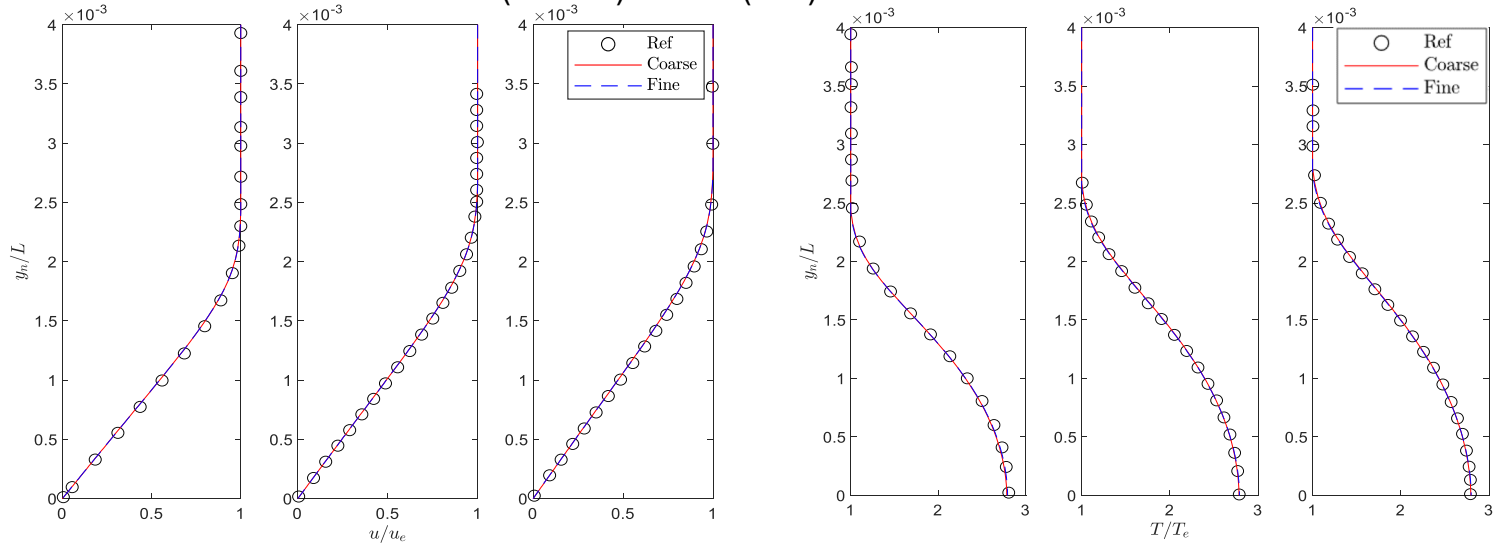

Fig 6. Velocity and temperature distribution in the wall normal direction at x^*/L=0.634, 0.76, and 0.825.

[6] Palacios, F., Economon, T. D., Aranake, A., Copeland, S. R., Lonkar, A. K., Lukaczyk, T. W., Manosalvas, D. E., Naik, K. R.,Padron, S., Tracey, B., Variyar, A., and Alonso, J. J., "Stanford University Unstructured (SU2): Analysis and Design Technology for Turbulent Flows,"52nd Aerospace Sciences Meeting, AIAA Paper No. 2014-0243, 2014

Parametric Study

Flow Conditions

Table. Nose radii (mm)

r_1	r_2	r_3	r_4	r_5	r_6	r_7	r_8	r_9	r_{10}
0.038	0.076	0.152	0.38	1.14	1.905	3.969	7.938	15.876	38.1

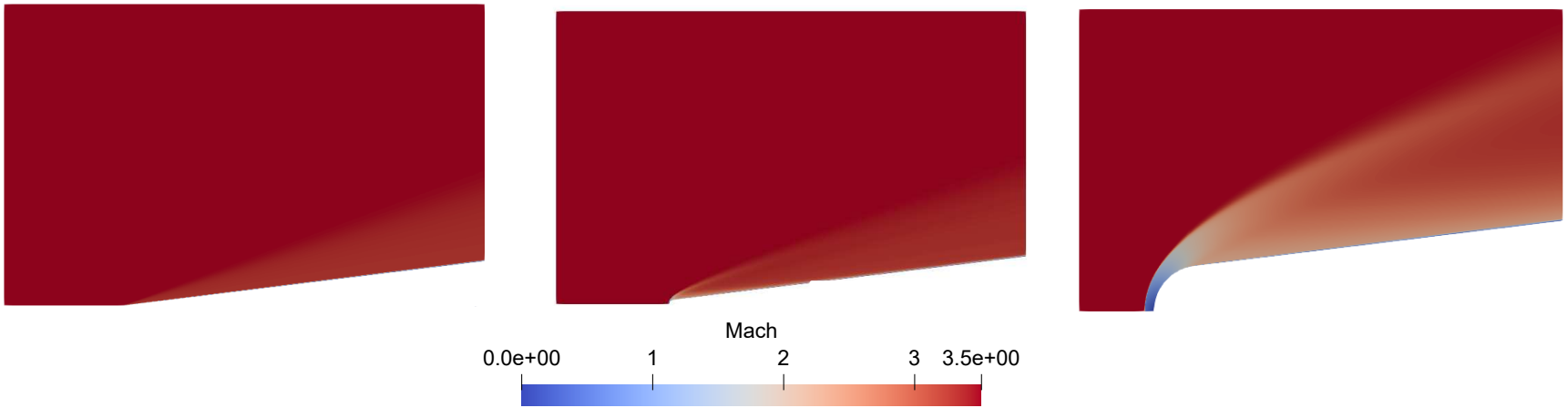

Fig 7. Mach contours of r_1, r_7, and r_{10} at $M_\infty = 3.50$.

Stability Validation

Eigenvalue

$$\left(A\frac{d^2}{dy^2}+B\frac{d}{dy}+C\right)\hat{\phi}=0$$

- Boundary conditions
  $y=0,\ \hat{\phi}_1=\hat{\phi}_2=\hat{\phi}_3=\hat{\phi}_5=0$
  $y\to\infty,\hat{\phi}_1,\hat{\phi}_2,\hat{\phi}_3,\hat{\phi}_5\to 0$
- Finite difference method
- Global method

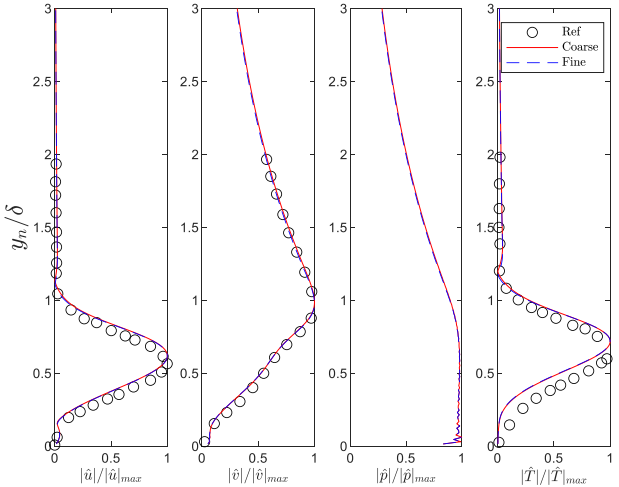

Fig 8. Eigenfunction comparison.

Table. Stability parameters

	r_1(mm)	f^*(kHz)	n	α(1/m)	ψ	u_p
Ref[7]	0.038	23.415	21	350.1-22.5i	N/A	N/A
LST	0.038	23.415	21	353.2-14.96i	65.93^o	0.64

[7] Mayer, C. S. J., "Numerical Investigation of the Nonlinear Transition Regime in Supersonic Boundary Layers," Ph.D. thesis, University of Arizona, 2009.

Stability Properties

➢ Maximum Growth Rate Distribution

Mack-mode: $0 < f^* < 75\text{kHz}, 0 < n < 40$

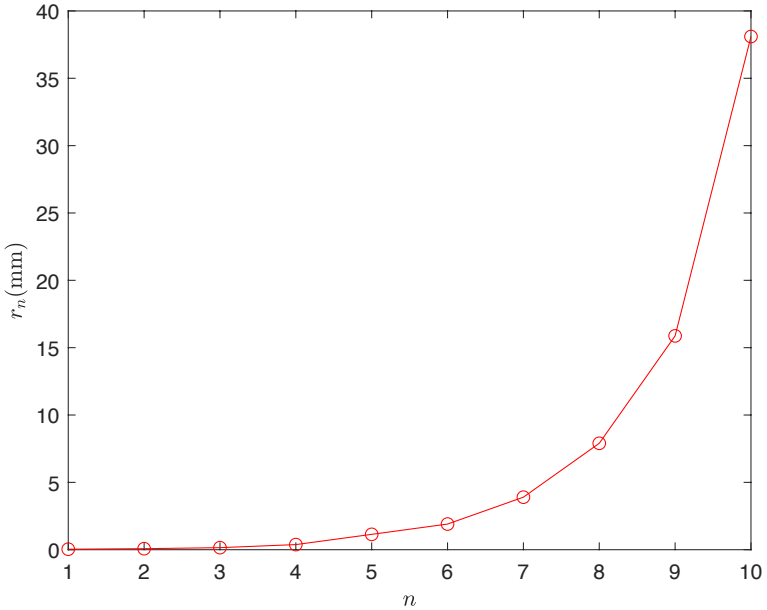

Fig 9. Nose radii distribution.

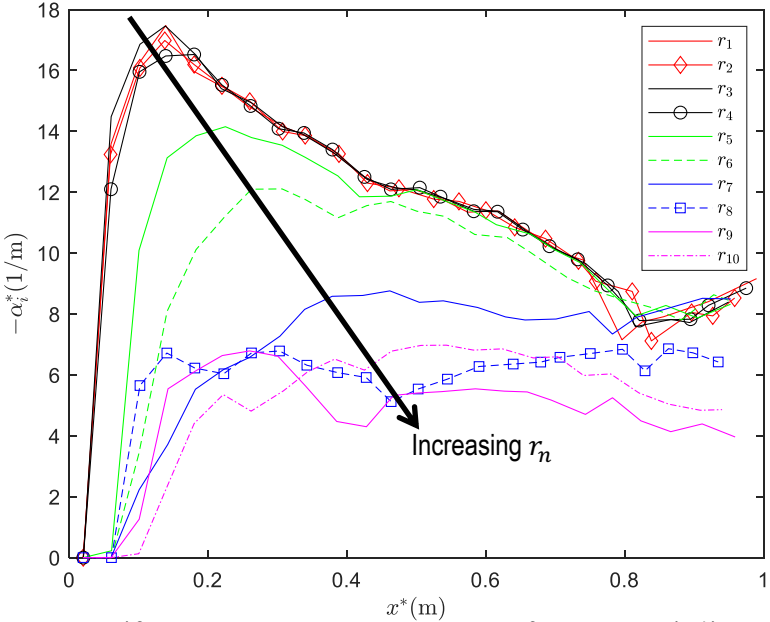

Fig 10. Maximum growth rates over all frequencies (f^*) and azimuthal mode number (n).

Single-Point Wall Pressure Spectrum

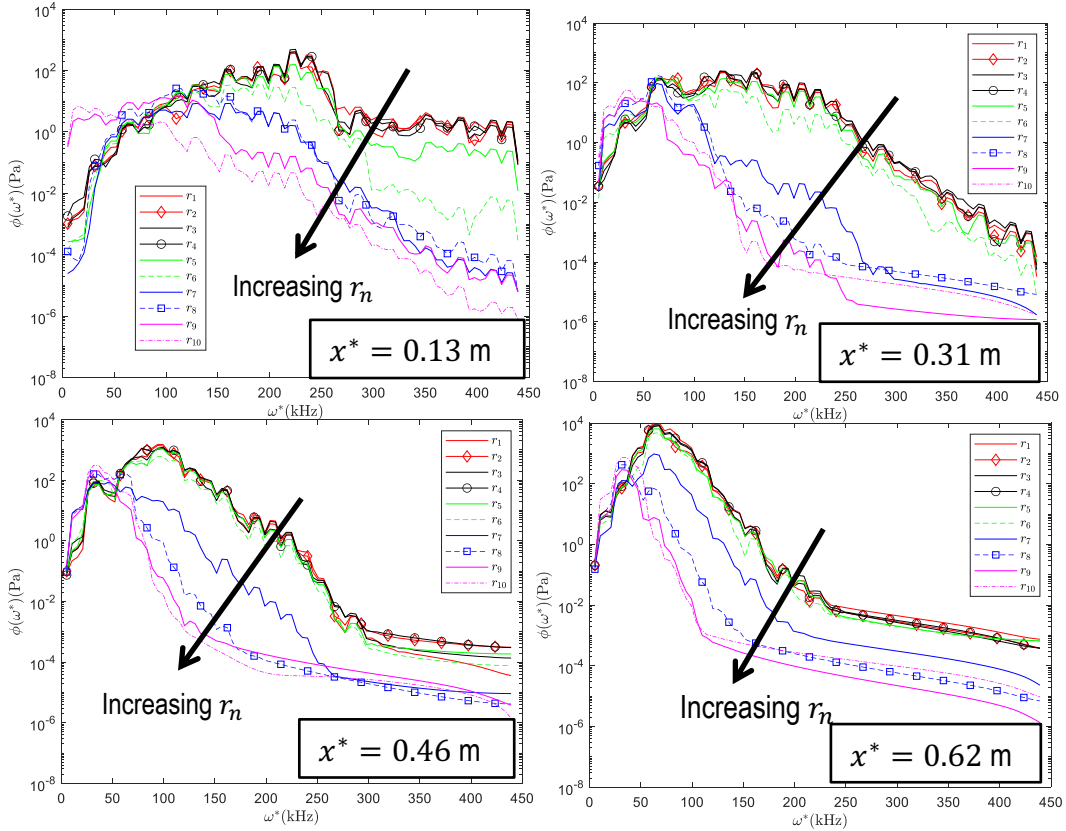

Wall Pressure Fluctuations

$$\tilde{p}(x,y,z,t) = \int_{-\infty}^{\infty} \hat{p}(y)\exp[i(\alpha x + \beta z - \omega t)]d\omega$$

- The value of $r_1 \sim r_4$ are close
- The maximum value of pressure spectrum is higher at downstream direction
- The value of pressure spectrum decrease as the nose radii increase ($r_4 \sim r_{10}$)

Spatial Coherence

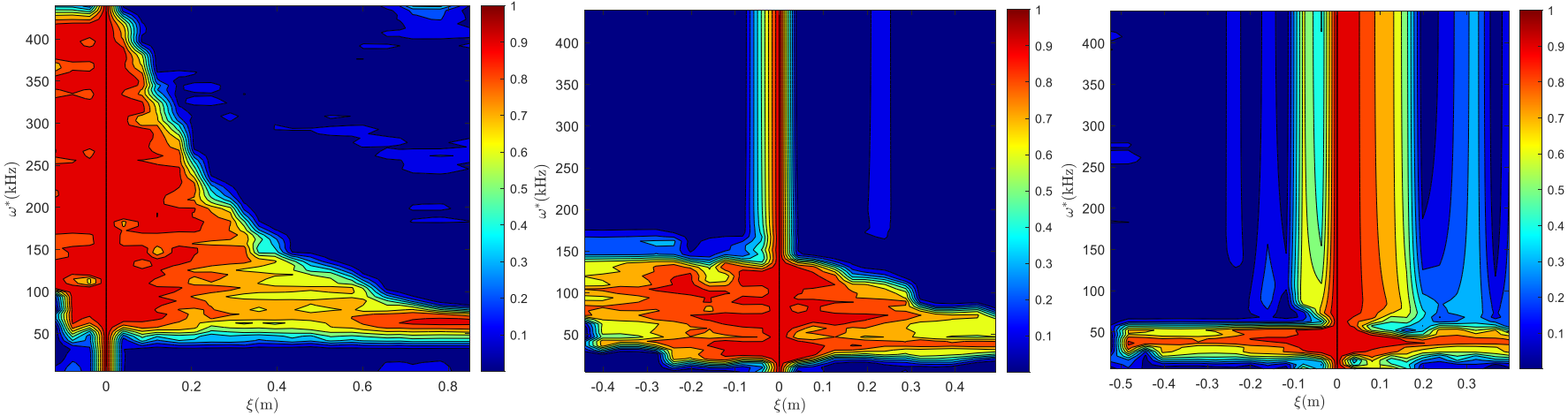

$r_1 = 0.038$ mm $\quad r_7 = 3.969$ mm $\quad r_{10} = 38.1$ mm

Fig 11. Spatial coherence of r_1, r_7, and r_{10} at $M_\infty = 3.50$, where the reference point of each case is the position of maximum growth rate in the streamwise direction.

- Amplified instability waves have higher spatial coherence
- Growth rates depend on the non-dimensional frequency $\omega = \frac{2\pi f^* l}{u_e^*}$ and $l = \sqrt{\nu_e^* x^* / u_e^*}$

Summary and Conclusion

- Summary and Conclusion
  - Steady flow-field for flow over cone are computed via SU2 and validated
  - The linear stability solver are validated and applied to compute the growth rate distribution
  - The single wall pressure spectrum and spatial coherence are shown
  - The small nose radii would not affect the maximum growth rate and pressure spectrum value; the large nose radii have smaller pressure spectrum value and have higher spatial coherence within a smaller frequency range

- Future Work
  - Add plasma actuator model (heating source) and study its effect on flow-field
  - Study the effects of Mach number on spatial coherence

Thank you

Jianhui Cheng: chengjianhui@ufl.edu
Steven A. E. Miller: saem@ufl.edu

AMERICAN INSTITUTE OF
AERONAUTICS AND ASTRONAUTICS